ICARUS 91, 14–28 (1991)

Dynamic Instabilities in Rotating, Low-Mass Protostars during Early Disk Formation

SHELBY YANG, RICHARD H. DURISEN, AND HOWARD S. COHL

Department of Astronomy, Swain West 319, Indiana University, Bloomington, Indiana 47405

AND

JAMES N. IMAMURA AND JOSEPH TOMAN

Institute of Theoretical Science and Department of Physics, University of Oregon, Eugene, Oregon 97403

Received May 14, 1990; revised October 25, 1990

We have recently constructed evolutionary model sequences for the equilibrium cores of rotating, low-mass protostars during their accretion phase. The cloud that collapses to form the core is assumed to be a pressure-supported, singular isothermal sphere in uniform rotation. The equilibrium core is assumed to be an isentropic, monatomic ideal gas. When $T/|W| \geq 0.1$, where T is the rotational kinetic energy and W is the gravitational potential energy, these core models represent the early disk formation stage. A linear stability analysis suggests that, for $T/|W| \geq 0.13$, the star/disk systems are dynamically unstable to nonaxisymmetric disturbances, with the fastest growth predicted for disturbances with four- or fivefold symmetry. By using one of our protostellar core models with $T/|W| = 0.157$ as the initial configuration in a three-dimensional hydrodynamics code, we have confirmed the dynamic instability of numerous multiarmed spiral disturbances. A disturbance with fourfold symmetry has the fastest growth rate and dominates in the linear regime. Swing amplification seems to be the mechanism that drives the dynamic growth. In the nonlinear regime, power shifts to threefold and then to twofold disturbances, but we do not detect any significant transport of mass or angular momentum nor any tendency for the disk to fragment by the end of a calculation spanning six and a half rotations. In one calculation, we also detect dynamic growth of a onefold disturbance. We conclude that fast-growing nonaxisymmetric instabilities set in as soon as Keplerian disks form during star formation, even when the disks have only limited radial extent.

1. INTRODUCTION

It has been confirmed observationally that young low-mass stars are commonly surrounded by disks of solar system size with masses up to a few tenths of $M_\odot$ (Beckwith *et al.* 1990, Beckwith and Sargent 1990). These disks are presumably Keplerian, as confirmed by observations in some cases (Sargent and Beckwith 1987). The disk phase usually lasts about 10^6 to 10^7 years (Strom 1990), and, in many cases, the falloff of the temperature with distance is less steep than expected for an accretion disk which has only local dissipation of gravitational energy. This suggests some form of "activity," such as nonlocal energy transport by waves (Adams and Shu 1986, Beckwith *et al.* 1990). Simultaneously, theorists have accumulated results which indicate that rapidly rotating disks and tori are susceptible to a wide range of hydrodynamic instabilities (see Adams and Lin 1990 and Sellwood 1989 for reviews). In this paper, we report that for star/disk systems built from the inside-out collapse of a centrally condensed cloud (Shu 1977, Cassen and Moosman 1981, Yuan and Cassen 1985, Shu *et al.* 1987, Durisen *et al.* 1989), the disks are dynamically unstable to nonaxisymmetric disturbances as soon as they begin to form.

From classical work on incompressible fluid ellipsoids, it is well known that rotating, self-gravitating equilibrium stars are subject to a variety of global secular and dynamic instabilities (Chandrasekhar 1969, Durisen and Tohline 1985). Some aspects of this classical work, particularly those concerning the barlike or two-armed Kelvin modes for oblate stars, have been tested by means of numerical three-dimensional hydrodynamic simultations, using rotating, self-gravitating polytropic fluids. A polytropic fluid has a power-law relation between pressure P and density ρ given by

$$P = K\rho^{1+1/n}, \tag{1}$$

where K and n are constants and n is called the "polytropic index." In these studies, the angular momentum distribution with mass is usually assumed to be

0019-1035/91 $3.00

that of a uniform-density sphere in solid body rotation, which is also the angular momentum distribution of a Maclaurin spheroid (see Section 2a). Just as for the incompressible Maclaurin spheroids, the first nonaxisymmetric dynamic instability encountered, as the rotation parameter $T/|W|$ (T = rotational kinetic energy, W = gravitational potential energy) increases along sequences of axisymmetric equilibrium polytropes, is the instability of global two-armed barlike modes for $T/|W| \geq 0.26$ (Tohline *et al.* 1985, Durisen and Gingold 1986, Durisen *et al.* 1986, Williams and Tohline 1987, 1988). These results, with n ranging from 0.5 to 1.8, have been argued to show that, as far as the lowest-order modes are concerned, the stability of rotating polytropic stars is insensitive to model details (Durisen and Tohline 1985). The numerical experiments with protostar-like configurations reported in this paper demonstrate, however, that this is not correct. Large-scale instabilities are quite sensitive to the choice of angular momentum distribution, even when n and $T/|W|$ are held fixed.

Consider an isothermal gas cloud in slow but uniform rotation which has undergone a protracted phase of ambipolar diffusion. Such a cloud will tend to acquire the density distribution of a singular isothermal sphere as a result of its subsonic evolution (see Shu *et al.* 1987 and references therein). If the equilibrium protostellar core formed by the collapse of a singular isothermal sphere retains the specific angular momentum distribution of its parent cloud, a slowly rotating, low-mass central star forms first with low $T/|W|$. As the inside-out collapse of the cloud proceeds, material with higher specific angular momentum falls in, so that $T/|W|$ increases monotonically and a nearly Keplerian disk eventually develops when $T/|W| \geq 0.1$ (Cassen and Moosman 1981, Yuan and Cassen 1985). Recently, we have computed a series of equilibrium $n = 3/2$ polytrope models that have the angular momentum distribution of a uniformly rotating, singular isothermal sphere (Durisen *et al.* 1989). These models are reasonably good approximations for rotating protostellar equilibrium cores during their accretion phase, when Stahler's (1988) interior entropies are adopted to account for accretion and deuterium burning. Using the Lagrangian normal mode equation (Lynden-Bell and Ostriker 1967) with trial eigen-functions appropriate for the Maclaurin spheroids, we have tested the linear stability of these models. We find that nonaxisymmetric instabilities set in for $T/|W| \geq 0.13$ and that the most unstable modes are of four- or fivefold symmetry. Using a modified version of J. E. Tohline's 3D hydrodynamics code (Tohline 1980, Williams 1988), we appear to have detected these dynamic instabilities in a protostellar core model with $T/|W| = 0.157$. In this paper, we shall describe these results in detail and propose a mechanism for the instabilities.

2. PREPARATION

a. Equilibrium Models

The gas cloud which collapses to form the equilibrium protostellar core is idealized as a singular isothermal sphere in uniform rotation. The rotation is dynamically unimportant at the cloud dimension, so it does not affect the initial equilibrium of the cloud or the initiation of the collapse. Each fluid element is assumed to conserve its angular momentum during the inside-out collapse of the cloud. Such local conservation of angular momentum guarantees that the distribution of specific angular momentum j as a function of cylindrical mass fraction $\mathcal{M}$ about the rotation axis is the same for the mass of a central sphere in the cloud and for that same mass after it collapses into the equilibrium core. The cylindrical mass fraction $\mathcal{M}(r)$ is defined as the fraction of the mass within a cylinder of radius r about the rotation axis. The $j(\mathcal{M})$ for a uniformly rotating, singular isothermal sphere has a unique functional form given by Eq. (4) of Durisen *et al.* (1989). The equation of state in the protostellar core is assumed to be well-approximated by an $n = 3/2$ polytrope, as justified in Stahler (1988).

Rotating protostellar core models are constructed using an axisymmetric equilibrium polytrope code (Bodenheimer and Ostriker 1973) based on the self-consistent field method (Ostriker and Mark 1968). The code is run with the same numerical accuracy as in Durisen (1975) and in Imamura *et al.* (1985). As demonstrated by Bodenheimer and Ostriker (1973), given a specific choice of polytropic index n and a unique functional form for $j(\mathcal{M})$, a one-parameter family of nondimensional models can be computed by setting the total mass M, the gravitatational constant G, and the K in Eq. (1) to unity and then varying the total angular momentum J, or equivalently $T/|W|$. A variety of functional forms for $j(\mathcal{M})$ can be obtained by considering the $j(\mathcal{M})$'s for uniformly rotating polytropic spheres with various choices for the polytropic index n' of the spheres (see Bodenheimer and Ostriker 1973). In this notation, the Maclaurin spheroid angular momentum distribution would be designated the $n' = 0\, j(\mathcal{M})$, and that of a uniformly rotating, singular isothermal sphere would be the $n' = \infty j(\mathcal{M})$. Model sequences can then be denoted by giving n and n' to specify the equation of state and the $j(\mathcal{M})$, respectively. A particular dimensionless model is denoted by specifying n, n', and $T/|W|$. As n' is increased for fixed n, more angular momentum is concentrated toward the equatorial mass elements so that models resembling stars with Keplerian disks occur at lower $T/|W|$. When $n = 3/2$ and $n' = \infty$, the sequence of models of

different $T/|W|$ represents protostellar cores at different evolutionary stages.

Figures 1a and b show the meridional density contours, the angular velocity distribution $\Omega(r)$, and the cylindrical mass fraction distribution $\mathcal{M}(r)$ for two protostellar core models ($n = 3/2$, $n' = \infty$) with $T/|W| = 0.056$ and 0.157, respectively. Also shown for comparison in Fig. 1b is the Keplerian $\Omega_K(r)$ for the $T/|W| = 0.157$ model, where $\Omega_K(r)$ is defined as the Ω required at r for a circular orbit about a point mass equal to $\mathcal{M}(r)$. For protostellar core models with $T/|W| \geq 0.1$ (see Durisen *et al.* 1989), the angular velocity Ω rises steeply to a maximum Ω_{max} from zero as r increases and then decreases to nearly Keplerian values. These models can be used to represent the early disk development phase of a protostar.

Although it is convenient to perform the stability analysis in dimensionless units for adiabatic perturbations, many readers would probably appreciate some feeling for the physical time scales and dimensions that characterize this problem. Sections IIb, IIIa, and the Appendix of Durisen *et al.* (1989) describe how to obtain physical units from the "polytropic units" ($G = M = K = 1$) of the model. The $T/|W| = 0.056$ model is not significantly different from the $T/|W| = 0.061$ model in Table 3 of Durisen *et al.* However, none of the models in Durisen *et al.* is close to the $T/|W| = 0.157$ model. We have, thus, in Table I, listed some of the useful parameters for the $T/|W| = 0.157$ model in both dimensional and dimensionless (polytropic) units. The parameters in dimensional units are obtained as follows. First, we assume the model is a member of an evolutionary sequence where the mass accretion rate $\dot{M}$ is $10^{-5}\ M_\odot$/year (corresponding to an isothermal cloud temperature = 34 K) and the deuterium-to-hydrogen ratio is 2.5×10^{-5}. Let us suppose that $M = 1M_\odot$. Figure A1 of Durisen *et al.* then gives $K = 1.16 \times 10^{15}$ in cgs units from Stahler's (1988) calculations. Using this K and Eq. (A1) of Durisen *et al.*, we then convert parameters from polytropic units to dimensional units. The total angular momentum J for this model in cgs units, as given in Table I, is 5.38×10^{51} g cm^{2}s^{-1}. Making use of the correct form of Eq. (3b)[1] of Durisen *et al.*, we find that to produce this much J in the inner $1M_\odot$ of a 34 K initial cloud, the angular speed of the precollapse isothermal cloud would have to be 4.2×10^{-15} radian s^{-1}, which is somewhat above the lower point d in Fig. 5 of Durisen *et al.* The equatorial radius of the model $R_{eq} = 19R_\odot$ is considerably smaller than the semimajor axis of Mercury's orbit ($83R_\odot$). If we take the nearly Keplerian $\Omega(r)$ to begin at $r/R_{eq} = 0.35$ (see Fig. 1b), the Keplerian disk contains about $0.16M_\odot$, so the disk is fairly massive, though small in radial extent. As discussed in Durisen *et al.*, this particular physical model would have already ignited deuterium. For the purpose of studying the stability of the star/disk system, we ignore this additional complication.

For $T/|W| = 0.157$, Fig. 1c shows the surface mass density Σ and midplane temperature T distributions as a function of r. The "disk" in our model is not an accretion disk and has distinctly steeper mass and temperature distributions than usually assumed for the equilibrium disks in other studies. For instance, $T(r) \propto r^{-5/2}$ and $\Sigma(r) \propto r^{-4}$ provide fits of about 15% accuracy over the range $r/R_{eq} = 0.3$ to 0.8, compared with $r^{-1/2}$ and $r^{-3/2}$, respectively, for the spatially extensive disks in Adams *et al.* (1989).

b. Linear Stability Analysis (LSA)

We have used a Lagrangian formulation of linear stability analysis for nonaxisymmetric modes (Lynden-Bell and Ostriker 1967) as a preliminary exploration of the stability characteristics of the protostellar core models. As a variational principle, this scheme accurately locates neutral points, where real eigenfrequencies of modes become zero (as in Imamura *et al.* 1985). In its current form, it provides only approximate results for dynamic instabilities, when eigenfrequencies are complex. We have applied the LSA code to the star/disk models in a manner that is equivalent to the tensor virial equations of order m for $e^{im\phi}$ disturbances (see Tassoul 1978), where ϕ is the azimuthal angle about the rotation axis. The LSA is equivalent to the tensor virial equations when the spatial part of the Lagrangian displacements of the fluid elements are taken to have the same form as the eigenfunctions of the Maclaurin spheroids, namely

$$\xi(r, \phi, z) \sim r^{m-1}\,(1, i, 0)\,e^{im\phi} \qquad (2)$$

in cylindrical coordinates. Because these are not true eigenfunctions unless $n = 0$ and $n' = 0$, the LSA is then merely an approximation of unknown accuracy.

The LSA analysis of models with a wide range of n, n', and $T/|W|$ values will be presented in detail elsewhere (Imamura *et al.* 1990). Table II shows the $T/|W|$ values above which the LSA predicts dynamic instabilities for various m when $n = 3/2$ and $n' = 0$, 1/2, 3/2, and ∞. Only modes with $m \leq 5$ were studied for this range of n'. For $n' = 0$, $m = 2$ is the first mode to become unstable, and higher m's become unstable at successively higher $T/|W|$'s. This pattern is the same for the $n = 0$, $n' = 0$ Maclaurin spheroids. Hydrodynamic calculations in 3D have verified many aspects of the $n' = 0$ results (Tohline *et al.* 1985, Durisen and Gingold 1986, Durisen *et al.* 1986, Williams and Tohline 1987). What is new in Table II is

[1] Equation (3b) of Durisen *et al.* (1989), which relates J and Ω_0, is incorrect. Its correct form should be $J = 0.0537\ G^{2/3}\ M^3\ \Omega_0/\dot{M}^{4/3}$. However, all tables and plots in that paper were based on the correct equation.

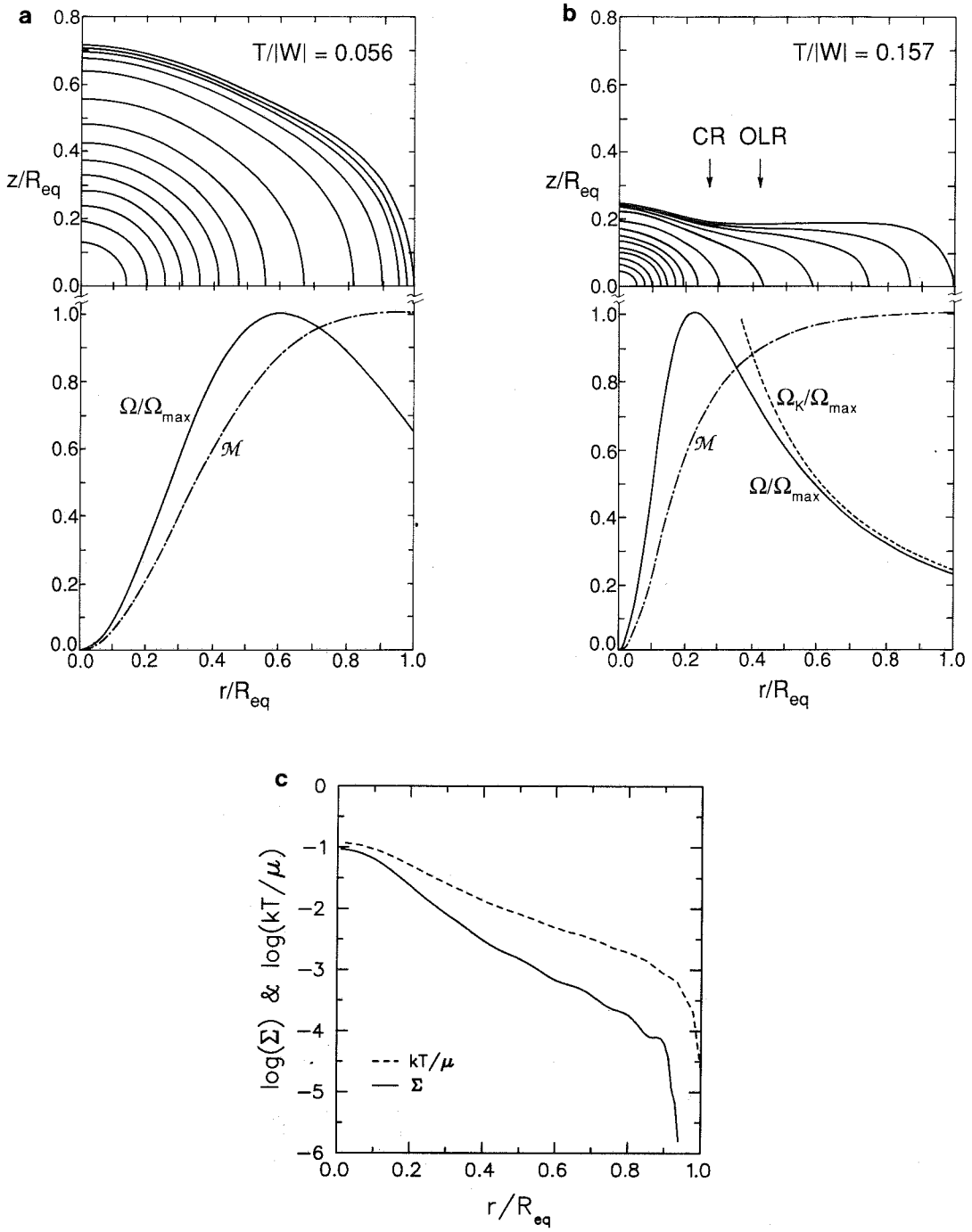

FIG. 1. (a) Equilibrium protostellar core model for $T/|W| = 0.056$. The upper panels give density contours in a meridional plane for $\rho/\rho_c = 0.9$, 0.8, 0.7, 0.6, 0.5, 0.4, 0.3, 0.2, 0.1, 3×10^{-2}, 10^{-2}, 3×10^{-3}, 10^{-3}, and the surface. The z axis is the rotation axis. The lower panels give $\Omega(r)$ normalized to Ω_{max} and cylindrical mass fraction $\mathcal{M}(r)$. (b) Equilibrium protostellar core model for $T/|W| = 0.157$. Also see the legend to (a). A Keplerian $\Omega_K(r)$ is shown for a circular orbit at r about a point mass $\mathcal{M}(r)$. The "CR" and "OLR" in the upper panel are the corotation radius and the outer Lindblad resonance, respectively, for the $m = 4$ pattern detected in the simulation. Small irregularities in $\Omega(r)$ near R_{eq} have been smoothed over. (c) Surface mass density Σ and the equatorial plane temperature T versus r/R_{eq} for $T/|W| = 0.157$. Both Σ and $kT/\mu = P/\rho$ are given in polytrope units, where k = Boltzmann constant and μ = average particle mass for the stellar gas. T is computed assuming the gas is ideal with a constant value of μ.

TABLE I
Physical Parameters for $T/|W| = 0.157$

Parameter	Dimensionless units	Physical units	Definition
J	0.632	5.38(51) g cm^2 s^{-1}	Total angular momentum
R_{eq}	9.60	19.1 $R_\odot$	Equatorial radius
R_{eq}/R_p	4.04	—	Ratio of equatorial to polar radius
ρ_c	0.0415	0.0312 g cm^{-3}	Central density
Ω_{max}	0.141	3.2(−5) radians s^{-1}	Maximum angular speed
$\mathcal{M}(\Omega_{max})$	0.649	0.649 $M_\odot$	Cylindrical mass at Ω_{max}
Ω_{eq}	0.030	6.7(−6) radians s^{-1}	Equatorial angular speed
v_{eq}	0.29	90 km s^{-1}	Equatorial velocity

that as n' increases, dynamic instabilities set in at markedly lower $T/|W|$'s and the ordering of the most unstable m values changes. For the $n' = \infty$, where we have studied m values up to 10, the LSA predicts that dynamic instabilities with $m = 5$ will set in first near $T/|W| = 0.13$ as $T/|W|$ is increased.

The functional form chosen for ξ contains a so-called trivial component for differentially rotating objects (Friedman and Schutz 1978). The trivial component fails to conserve circulation and amounts to a relabeling of fluid elements which destroys the gauge invariance of the energy functional. Our LSA approach is thus, in a strict sense, invalid. A priori, however, one cannot predict to what extent and in what sense trivials affect the results of stability analyses. We note that in analyses of the neutral points of the protostellar core models and other polytropic sequences where the effects of the trivials could be eliminated, trial functions such as Eq. (2) lead to qualitatively correct results (Imamura *et al.* 1985). Thus, the LSA in its tensor virial equation form has proven to yield surprisingly accurate results in situations in which its accuracy could be checked.

TABLE II
$T/|W|$ for Onset of Dynamic Instability According to the LSA

n'	$m = 2$	$m = 3$	$m = 4$	$m = 5$
0	0.260	0.280	0.292	0.299
1/2	0.254	0.254	0.252	0.252
3/2	—	—	(0.175)	0.164
∞	(0.20)	0.148	0.133	0.132

Note. Blank entries indicate that equilibrium models of large enough $T/|W|$ could not be converged. Entries in parentheses are given for a few such cases where the stability limit could be extrapolated with some confidence. All entries are for $n = 3/2$ polytropes.

c. 3D Hydrodynamics Code

The 3D code used is a version of Tohline's (1980) hydrodynamics code with self-gravity modified to include second-order van Leer monotonic advection and operator splitting (Norman and Winkler 1986, Williams 1988). The hydrodynamic and Poisson equations are solved by a finite-difference method on a cylindrical grid (r, ϕ, z). The hydrodynamic structure is advanced in time through an explicit, first-order time integration of the equations. Different but uniform grid spacing is used in the three cylindrical coordinates; and spatial gradients are differenced in a second-order accurate form. As in Williams (1988), all quantities are located at cell centers. Reflection symmetry about the equatorial plane is assumed; hence the calculations are performed only for the upper hemisphere, using a $32 \times 64 \times 16$ cylindrical grid. Tests described in the Appendix show that this code causes significantly less numerical damping of nonaxisymmetric structure than Tohline's original code.

3. HYDRODYNAMIC SIMULATIONS

a. Three Simulations

According to the LSA prediction, our protostellar core models are unstable to high-order nonaxisymmetric disturbances once $T/|W| \geq 0.13$. To test this, two equilibrium models with $T/|W| = 0.056$ and 0.157 are selected from our model sequence. The models are chosen so that their $T/|W|$ is either well above or far below the critical value 0.13. To stimulate nonaxisymmetric disturbances, both axisymmetric equilibrium models are given low-level, random density perturbations after they are mapped onto the three-dimensional grid, such that $\delta\rho/\rho$ in every cell is a random number between -5×10^{-3} and 5×10^{-3}. The models are then followed for several rotations. The results of the simulations are summarized in Table III.

TABLE III
Hydrodynamic Simulations for $n' = \infty$

$T/\|W\|$	Number of rotations	$m = 1$	Outcome
0.056	2.2	On	Nonaxisymmetric disturbances damp slowly.
0.157	4.4	On	Multiarmed disturbances grow in the linear regime; $m = 1$ dominates later.
0.157	6.5	Off	Multiarmed disturbances grow in the linear regime with $m = 4$ dominant; power shifts to $m = 3$ and $m = 2$ in the nonlinear regime.

Disturbances with cos ϕ and sin ϕ symmetry are artificially suppressed in one of the $T/|W| = 0.157$ calculations, because, when they are not, the center of mass of the whole system drifts as the $m = 1$ nonaxisymmetric disturbance grows. Such a drift is completely unphysical. Although the $m = 1$ disturbance starts to grow before the center of mass drifts significantly, suggesting that the growth of $m = 1$ may be real, we are more confident about resolving the behavior of the higher m-value disturbances if the center of mass is held fixed. Consequently, all of the details presented in this section for $T/|W| = 0.157$ are from the calculation with $m = 1$ suppressed. However, based on a comparison of the two calculations, we find that the linear regime results for $m = 3$, 4, and 5 are not strongly affected by the suppression of $m = 1$.

b. Method of Analysis

To measure the growth of disturbances with different symmetry, we employ a method used by Tohline *et al.* (1985). The azimuthal density distribution at each meridional grid location is Fourier transformed to get

$$a_m(r, z) = \frac{2}{\pi} \sum_{L=1}^{64} \rho(r, \phi, z) \cos(mL\delta\phi)\delta\phi \qquad (3a)$$

TABLE IV
Comparison of LSA and Hydrodynamic Results for $T/|W| = 0.157$

	t_e		Ω_p	
m	Hydro	LSA	Hydro	LSA
3	22	35	0.133	0.0474
4	21	19	0.134	0.0434
5	25	20	0.129	0.0410

Note. t_e and Ω_p are given in polytrope units where $G = M = K = 1$. In the same units, $\Omega_{max} = 0.141$ for the $T/|W| = 0.157$ protostar model generated by the equilibrium code.

and

$$b_m(r, z) = \frac{2}{\pi} \sum_{L=1}^{64} \rho(r, \phi, z) \sin(mL\delta\phi)\delta\phi \qquad (3b)$$

where $\delta\phi = 2\pi/64$ is the grid spacing in ϕ and m takes on the values $m = 0, 1, 2, \ldots, 31$ for a_m and $m = 1, 2, 3, \ldots, 32$ for b_m. The amplitude c_m and phase angle ϕ_m of Fourier component m are calculated according to

$$c_m(r, z) = [a_m(r, z)^2 + b_m(r, z)^2]^{1/2} \qquad (4a)$$

and

$$\phi_m(r, z) = \arctan[-b_m(r, z)/a_m(r, z)]. \qquad (4b)$$

The relative amplitude $A_m(r, z) = c_m/c_0$ as a function of time then provides a measure of the growth rate for nonaxisymmetric disturbances of azimuthal order m. The phase ϕ_m as a function of time is used to determine the emergence of a coherent disturbance with a fixed pattern speed $\Omega_p = \dot{\phi}_m/m$.

No growth occurs in the $T/|W| = 0.056$ calculation after two rotation periods. In fact, the A_m's generally decrease as discussed in the Appendix. In the $T/|W| = 0.157$ calculations, growth is evident after the same number of rotations, so the $T/|W| = 0.157$ calculations are continued over an extended period.

c. Linear Regime for $T/|W| = 0.157$

Figures 2 and 3 show the amplitudes A_2, A_3, A_4, A_5, and the phase ϕ_4 as a function of time at the radius $r/R_{eq} = 0.27$ in the equatorial plane. Time is measured in these plots in units of the fluid rotation period of the equilibrium model at Ω_{max}. This period is 45 in polytropic time units. We have carefully examined similar plots of A_m and ϕ_m throughout the equatorial plane for m up to 10. The emergence of a coherent disturbance is determined by the detection of a sinusoidal pattern in the cos ϕ_m plots. For a well-defined dynamic instability, coherent pattern rotation should emerge at about the same time as the onset of exponential growth in the corresponding A_m. These criteria are met by $m = 3$, 4, and 5 in the linear regime for the region just outside the radius of Ω_{max} (see Fig. 5), so we are reasonably confident that we have detected linear dynamic instabilities for these m's. The $m = 2$ disturbance also grows in amplitude, but there is not a well-defined exponential phase, and ϕ_2 does not exhibit a coherent pattern. Coherent pattern rotation and exponential growth with similar Ω_p and e-folding time t_e are seen for $m = 4$ throughout the region $r/R_{eq} = 0.23$ to 0.43. The onset is at about the same evolutionary time over these r's for $m = 4$ and is somewhat earlier than for $m = 3$ and 5. Coherence

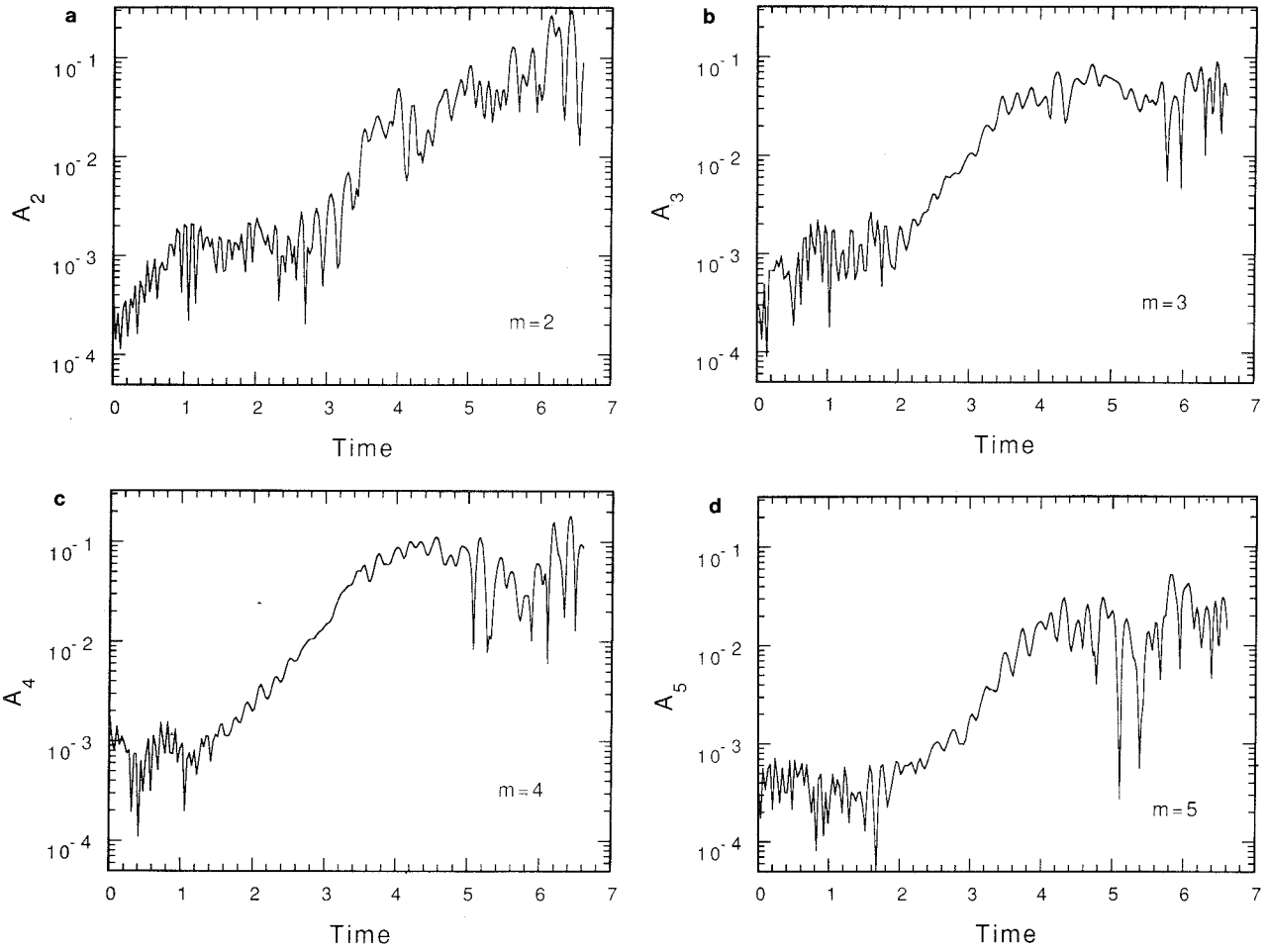

FIG. 2. Fourier amplitudes of $\delta\rho/\rho$ versus time for (a) $m = 2$, (b) $m = 3$, (c) $m = 4$, and (d) $m = 5$ at $r/R_{eq} = 0.27$ in the equatorial plane. Time is given in units of 45 polytropic units, which is approximately the rotation period at Ω_{max}. Only data from every 50th hydro time step are plotted.

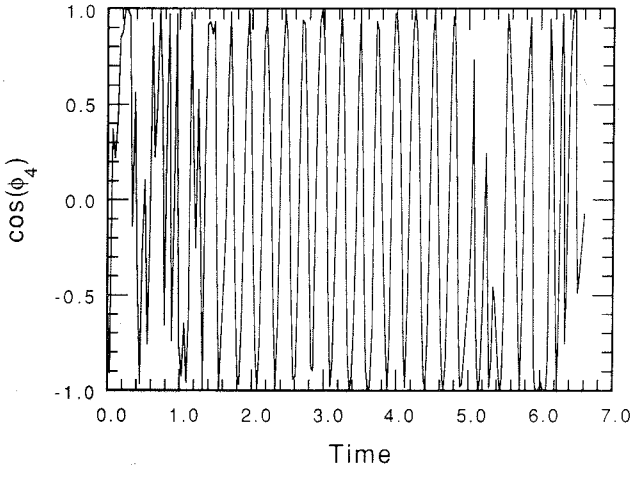

FIG. 3. Cosine of the Fourier phase for $m = 4$ at $r/R_{eq} = 0.27$ in the equatorial plane. Note the emergence of a regular sinusoidal pattern at $t = 1.5$, corresponding to the beginning of the exponential growth of A_4 in Fig. 2c. Only data from every 50th hydro time step are plotted.

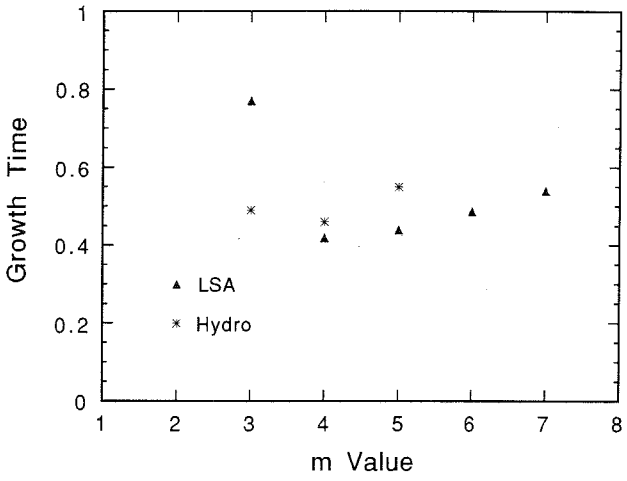

FIG. 4. Comparison of exponential growth times t_e between the hydrodynamic calculation and the LSA. Times are given in units of 45 polytropic time units, which is approximately the rotation period at Ω_{max}.

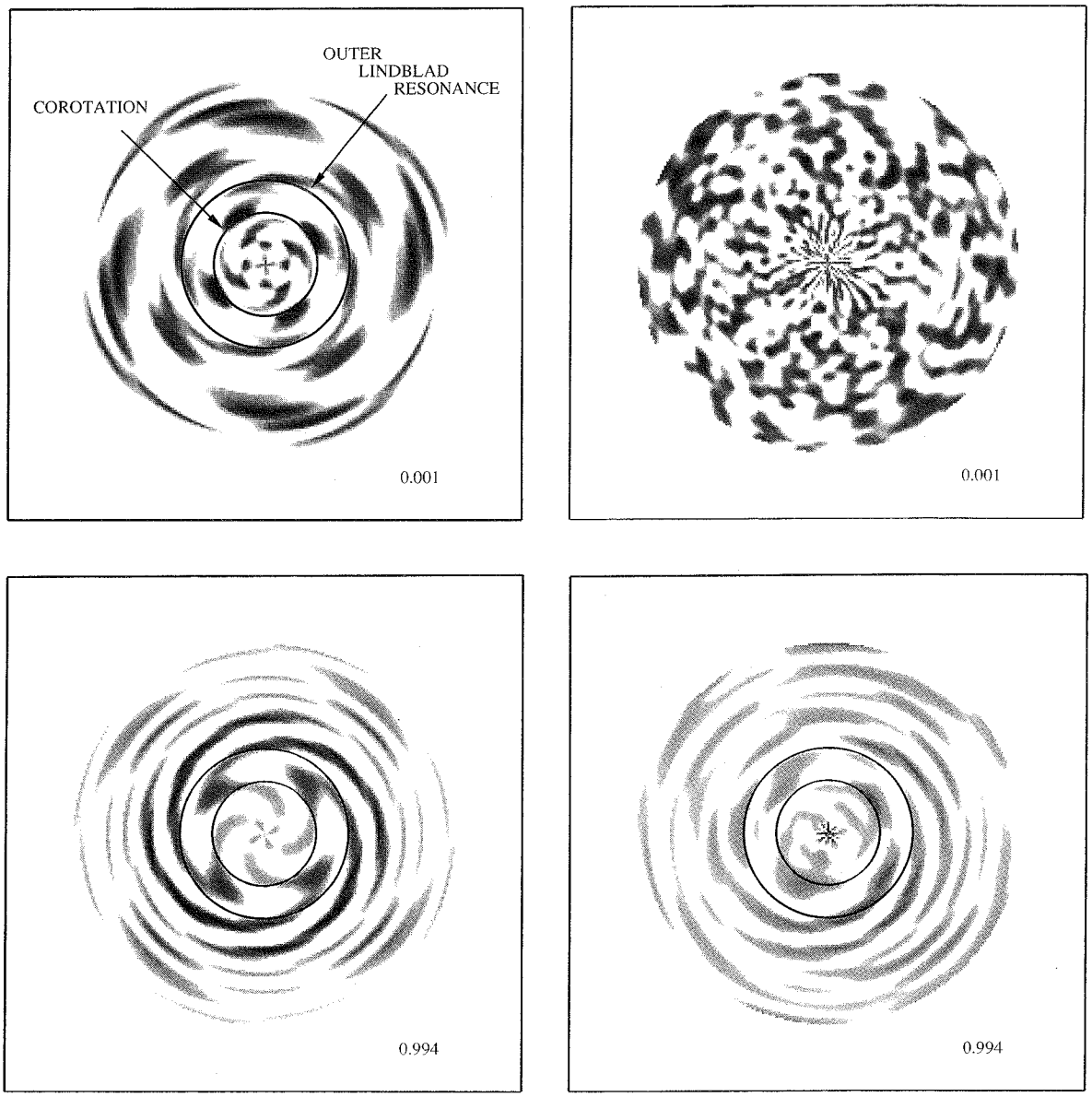

FIG. 5. Gray-scale plots of nonaxisymmetric $\log(\delta\rho/\rho)$ in the equatorial plane at various evolutionary times. Two panels are shown at each of seven times. The left-hand panel is for $m = 4$ alone; the right-hand panel is the full nonaxisymmetric $\delta\rho/\rho$. For contrast, all $\delta\rho/\rho$ less than 10^{-4} are set to white. The radii correspond to the corotation and outer Lindblad resonances for $m = 4$. The gray scale in each plot is normalized to the maximum value of $\delta\rho/\rho$ in that plot. Rotation is counterclockwise. Time is given in the lower right in units of rotation periods at Ω_{max}.

in ϕ_3 and ϕ_5 is more restricted in radial extent. The $m = 4$ disturbance is the dominant coherent disturbance in the linear regime. Higher m values typically show growth in A_m and coherence in ϕ_m much later in the calculation, if at all. We suspect their growth is due to power from lower m values being fed into that of higher m values by nonlinear effects.

Figure 4 and Table IV compare Ω_p and t_e from the hydrodynamic simulations with the LSA approximate predictions for $m = 3$, 4, and 5. It is startling that the t_e's agree well, while the Ω_p's disagree badly. Since the Maclaurin spheroid eigenfunctions used in the LSA have large amplitudes at large r/R_{eq} where Ω is low, it is not surprising that the LSA Ω_p's are lower than those seen in the hydro code. However, it is remarkable that the LSA can successfully predict dynamic instabilities which actually grow with a very different Ω_p. We shall return to this point in Section 4b. From the discussion in the Appendix, we expect $m \geq 5$ disturbances to be affected, if not suppressed, by numerical diffusion. We cannot determine

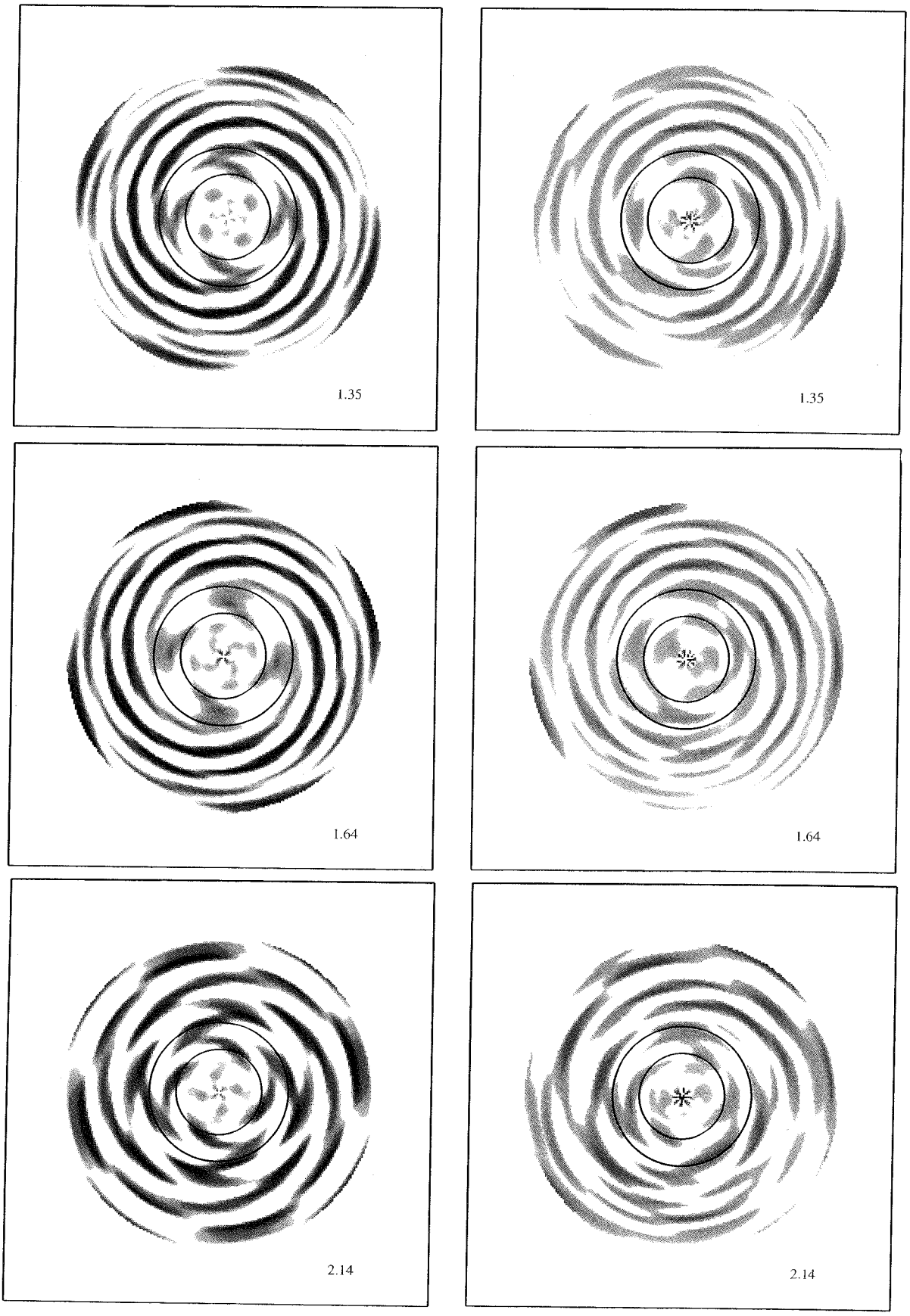

FIG. 5—*Continued*

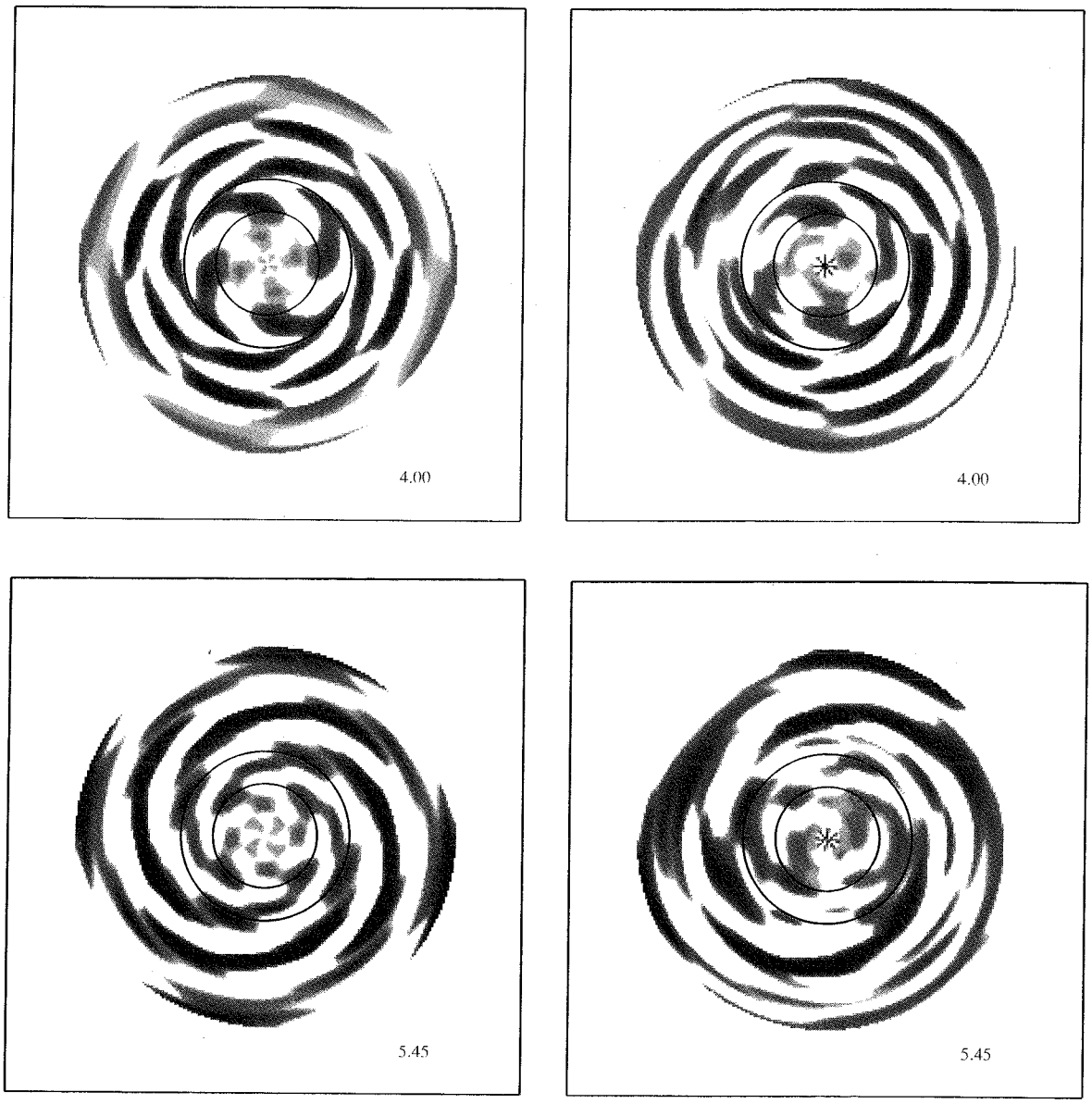

FIG. 5—*Continued*

with the present hydro code at this resolution whether or not modes with $m \geq 5$ may actually grow faster than those with $m = 4$.

d. Equatorial Plane Images for $T/|W| = 0.157$

In the linear regime, a four-armed disturbance dominates for about three rotations. After the disturbance becomes nonlinear, its amplitude saturates at about 10 to 20% in $\delta\rho/\rho$. Later, Fourier power shifts to disturbances with lower symmetry. To illustrate these features of the evolution, Fig. 5 shows a series of gray-scale plots of $\log(\delta\rho/\rho)$ in the equatorial plane both for $m = 4$ and for the full nonaxisymmetric disturbances. To enhance the contrast, values of $\delta\rho/\rho$ below 10^{-4} are set to white. To be more precise, we have plotted, for $m = 4$,

$$\log(\delta\rho/\rho) = \log\{A_4(r, 0)\cos[4\phi + \phi_4(r, 0)]\}, \quad (5)$$

and, for the full nonaxisymmetric plots,

$$\log(\delta\rho/\rho) = \log\left\{\sum_{m=2}^{32} A_m(r, 0)\cos[m\phi + \phi_m(r, 0)]\right\}, \quad (6)$$

when the arguments of the logarithms are $\geq 10^{-4}$. Note that only relative densities are shown and the axisymme-

tric parts are left out. This permits arbitrarily small nonaxisymmetric disturbances to be displayed clearly.

The corotation resonance (CR) and the outer Lindblad resonance (OLR) for $m = 4$, plotted as the two concentric circles in Fig. 5, are defined, respectively, by

$$\Omega_p = \Omega, \tag{7}$$

which occurs at $r/R_{eq} \approx 0.23$ for $m = 4$, and

$$\Omega_p = \Omega + \kappa/m, \tag{8}$$

which occurs at $r/R_{eq} \approx 0.42$ for $m = 4$. The value of Ω_p for $m = 4$ is determined from the phase $\phi_4(t)$, and $\Omega(r)$ and $\kappa(r)$ are determined from the equilibrium model. The quantity κ, the epicyclic frequency (see Binney and Tremaine 1987), is

$$\kappa^2 = r\frac{d\Omega^2}{dr} + 4\Omega^2. \tag{9}$$

As can be seen from the plots, after one rotation period, the four-armed disturbance has established a well-defined pattern with short-wavelength trailing spiral waves outside the OLR and what can be interpreted as pieces of long-wavelength leading and trailing spiral waves between the CR and the OLR. The lumpy structure of the short trailing waves is probably the result of interference between leading and trailing short waves. This pattern persists from $t = 1$ to 2 until the interference between the short leading and short trailing waves becomes so strong that the pattern shatters into arcs and lumps. Wave patterns following this stage are more complicated, continuously changing, and hard to identify. However, a coherent pattern speed is maintained in the region bounded by the CR and the OLR during exponential growth, which ends at $t \approx 3.5$, and during the early nonlinear phase from 3.5 to 4.5. Comparison of the left- and righ-hand panels of Fig. 5 shows that, in the exponential growth regime, represented by the $t = 1.35$ to 2.14 panels, and, in the early part of the nonlinear regime, as represented by the $t = 4.00$ panels, $m = 4$ dominates the appearance of the nonaxisymmetric structure even though other m values are present with substantial amplitude. In the late nonlinear regime, as represented by the $t = 5.45$ panels, it is evident that there is more power in the $m = 2$ and 3 distrubances than in the $m = 4$. This can also be seen, to some extent, by direct comparison of the A_m's in Fig. 2.

e. Asymptotic Behavior

We have not yet determined the ultimate nonlinear outcome of the dynamic instabilities. No consistent behavior emerges. Equatorial plane patterns for individual m values continuously change and seem to exhibit both leading and trailing spiral behavior, usually with indications of strong interference between leading and trailing waves. As discussed in the Appendix, we have detected no significant changes in either the axisymmetric mass distribution $\mathcal{M}(r)$ or the angular momentum distribution $j(\mathcal{M})$. We have also used the A_m's as nonlinear time series data and analyzed them for chaotic behavior without success.

The only noticeable trend is the shift in nonaxisymmetric power to $m = 2$. By the end of the calculation, the $m = 2$ amplitude in $\delta\rho/\rho$ reaches 20 to 30%. At some radii, as in Fig. 2a, there is a suggestion that $m = 2$ is still growing. Whether this leads to disk fragmentation or net transport remains to be seen through longer calculations. We should add that when $m = 1$ disturbances were not suppressed, power shifted to $m = 1$ in the nonlinear regime, but we do not have complete confidence in this result because of the simultaneous drift of the center of mass.

4. DISCUSSION

a. Swing Amplification as the Instability Mechanism

The equatorial plane patterns present during the exponential growth of $m = 4$, as illustrated by the left panels for $t = 0.994$, 1.35, 1.64, and 2.14 in Fig. 5, suggest that the dynamic instability mechanism is swing amplification (see Binney and Tremaine 1987 and references therein). As mentioned in Section 3d, it is possible to identify all the components of a four-wave feedback loop, including pieces of long leading and trailing waves in the regime between the CR and the OLR, a trailing short wave propagating to the disk edge outside the OLR, and hints, in the lumpiness and especially near the edge, of a short leading wave reflected by the edge and propagating inward. At $t = 2.14$, the breakup of the pattern outside the OLR into leading and trailing arcs seems to suggest strong interference between the short leading and trailing waves. As swing amplification involves the feedback of short leading waves (see Adams *et al.* 1989 and references therein), we conclude that swing amplification is the driving mechanism.

The radial wavelength of the density waves can be calculated using the WKBJ dispersion relation for a gaseous disk (see Binney and Tremaine 1987),

$$m^2(\Omega - \Omega_p)^2 = \kappa^2 - 2\pi G\Sigma|k| + k^2 v_s^2, \tag{10}$$

where v_s is the adiabatic sound speed, k is the radial wavenumber, and Σ is the surface mass density. This relation gives wavelengths $\lambda = 2\pi/|k|$ for the $m = 4$ short waves (the greater solutions for $|k|$), in agreement with our hydro results to within 25% at $r/R_{eq} = 0.6$ and 10%

at $r/R_{eq} = 0.8$. The agreement suggests that the WKBJ treatment is reasonably accurate for the outer nearly Keplerian part of our star/disk system, and it again supports our identification of the linear regime patterns outside OLR as short trailing density waves.

Swing amplification has been most extensively studied for thin gaseous and stellar disks with flat rotation curves, resembling galaxies. As presented in Toomre (1981), for $m = 2$ disturbances, strong amplification in such disks requires that the X and Q parameters, defined by

$$Q = \frac{v_s \kappa}{\pi G \Sigma} \tag{11}$$

and

$$X = \frac{r\kappa^2}{2\pi m G \Sigma}, \tag{12}$$

must satisfy $X < 3$ and $Q < 3$ near the CR. For $m = 4$ in the $T/|W| = 0.157$ model, where both Q and X increase monotonically with cylindrical radius, the Q and X conditions are satisfied for $r/R_{eq} < 0.64$. X and Q values at the CR are 0.44 and 1.4, respectively.

As reviewed in Adams and Lin (1990) and in Papaloizou and Savonije (1989) [see also Miyama *et al.* (1984), Hachisu *et al.* (1988), Vishniac and Diamond (1989), and Boss (1989) for work not cited in these reviews], various types of nonaxisymmetric instabilities in self-gravitating gaseous disks and tori have been reported by other researches. It goes beyond the scope of this paper to discuss and evaluate all the associated mechanisms. In most cases, the disks are thinner and more spatially extended than ours and the central mass is not included explicitly in the analysis. The evidence described in the preceding paragraphs, although not conclusive, indicates that our calculations satisfy many of the necessary conditions for the swing mechanism to operate. Code improvements suggested in Section 4e, especially for the LSA, should allow us to delineate the physical mechanism of instability with greater confidence in the near future.

b. Comparison of LSA and Hydro Code Results

In some respects, it is remarkable that, with the nonspiral trial Lagrangian displacements of Eq. (2), the LSA appears to detect the proper m's and t_e's of spiral density wave instabilities driven by swing amplification. We are currently examining both the LSA and hydro code results in more detail in an effort to understand this. The trial ξ clearly concentrates amplitude toward R_{eq}, so it is not surprising that the LSA predicts much slower pattern speeds. For $m = 4$, Ω_p(LSA) in Table IV corresponds to Ω at $r/R_{eq} = 0.82$. When we examine the terms in the LSA which determine whether or not an imaginary part of the eigenfrequency will occur, leading to exponential growth, we find that the imaginary part is generated entirely in the region between $\Omega = \Omega_p$(LSA) and the disk edge. This suggests that the entire disk, not just the region near Ω_{max}, may be susceptible to dynamic instabilities due to swing amplification with a wide range of pattern speeds. The trial function in the LSA, being weighted strongly toward large r, selects an Ω_p that produces a resonant cavity near the edge of the disk. The hydro code, on the other hand, may find growth of disturbances with Ω_p near Ω_{max}, because, close to Ω_{max}, the disk has the lowest Q. We are currently developing a more accurate LSA which should clarify some of these questions and determine the m and $T/|W|$ for onset of instability along the model sequence with more precision.

c. m = 1 Spiral Modes

Independent work by other researchers (Adams *et al.* 1989, Shu *et al.* 1990) has demonstrated that a mechanism related to swing amplification can destabilize one-armed spiral modes in massive and spatially large Keplerian disks around stars. They call this mechanism "sling" amplification, because an indirect potential term induced by the displacement of the star (treated as a point mass) from the center of mass of the system plays an indispensible role in the amplification. The instability involves a four-wave feedback loop which is somewhat similar to the one we have discussed for swing amplification. The work by this group is so far limited to characterization of the instability in the linear regime. The $m = 1$ character raises the possibility that the nonlinear outcome could be the production of a binary companion from the disk.

In fact, when we permit $m = 1$ disturbances in our own hydro calculations, they do eventually dominate in the nonlinear regime. We saw such behavior even in preliminary calculations from the summer of 1988 (Yang and Durisen 1989). Unfortunately, we cannot trust this result, because just after $m = 1$ begins its exponential growth, the center of mass begins an exponential deviation from the grid center. By the end of the $m = 1$ "on" calculation for $T/|W| = 0.157$, the $m = 1$ disturbance is at about 10% amplitude in $\delta\rho/\rho$ and the center-of-mass deviation is 0.7% of the equatorial radius or 16% of the radial grid spacing. This deviation is not large, but is growing exponentially. We intend to find a way to treat $m = 1$ more accurately. At this point, we can only report that an $m = 1$ disturbance in $T/|W| = 0.157$ does grow and that the $T/|W| = 0.157$ model does have an extended enough Keplerian disk to include the resonant cavity necessary for the sling mechanism to work (Adams *et al.* 1989).

d. Model Improvements

One problem with our protostar models is that we effectively apply the same internal specific entropy to our high

$T/|W|$ models as Stahler (1988) would assign to a nonrotating protostellar core of the same mass (Durisen *et al.* 1989). When the accretion flow misses the starlike, slowly rotating, central body for $T/|W| \geq 0.1$, the Keplerian disk in our model is probably assigned too large a specific entropy and so is too hot and thick. However, this casts no doubt on our demonstration of dynamic instability. For both swing and sling amplification, the lower Q's expected in lower entropy models would only tend to enhance instability (Toomre 1981, Shu *et al.* 1990). We plan, in future studies, to produce models with lower disk entropy by using a nonpolytropic P–ρ relation.

The $n' = \infty$ $j(\mathcal{M})$ produces the steep rise to Ω_{max} in the starlike part of the model. For plausible initial rotation rates of the cloud out of which the protostar forms (see Section 2a), the "star" would be expected to have ignited deuterium and be in uniform rotation before the disk forms (Durisen *et al.* 1989). By conventional theory, there would then be an even steeper change in Ω between star and disk over a thin boundary layer. We cannot say at present whether such changes in the form of $\Omega(r)$ would affect the instability. Although we describe a four-wave feedback loop using reflection of short waves at the disk edge, we cannot rule out a contribution to the feedback from waves transmitted through the starlike part of our model. We need to test the sensitivity of the instability to the form of $\Omega(r)$ and to the nature of the star/disk boundary.

Another serious concern is that the feedback loop, as we currently understand it, requires propagation of waves across the disk and strong reflection at the outer edge. The sensitivity of the instability to these effects needs to be tested. The sharp outer edge of our model disk may be realistic only during the earliest phase of disk development, when the accretion streamlines first begin to miss the central star.

e. Code Improvements

Efforts are underway to improve both the LSA and the hydro codes. Two of us (J.N.I. and J.T.) are developing a hydrodynamic code linearized about equilibrium, which should permit accurate study of waves, feedback loops, and dynamically growing disturbances. Another two of us (S.Y. and R.H.D.) are exploring alterations in the nonlinear hydro scheme to improve numerical performance and to permit finer grid resolution at affordable expenditures of computer time. For instance, we have already found that implementation of a second-order time differencing scheme developed by Christodoulou and Tohline (1990) permits larger time steps and that adoption of cell face centering cures the sawtooth discussed in the Appendix.

5. CONCLUSIONS

Both the LSA and 3D hydro calculations have shown that for $T/|W| \geq 0.13$, star/disk models for the equilibrium cores of low-mass protostars are dynamically unstable to multiarmed nonaxisymmetric modes. Growth times estimated from both methods agree reasonably well. Disturbances with fourfold symmetry have the fastest hydro code growth rates in the linear regime. The mechanism for the growth of disturbances seems to be swing amplification of spiral density waves through a four-wave feedback loop.

For star formation, this leads to a conclusion of considerable importance. When low-mass protostars form by inside-out collapse of singular isothermal spheres, the resulting massive disks are susceptible to violent nonaxisymmetric instabilities even as they just begin to form. Our work shows that swing amplification produces multiarmed spiral disturbances; the work of others (Adams *et al.* 1989, Shu *et al.* 1990) demonstrates a related sling instability of one-armed modes, which we also seem to detect. The nonlinear consequences of these instabilities remain to be determined. Our calculations so far indicate a nonlinear trend toward saturation of the high-m modes but with continued growth of low-order disturbances ($m = 1$ and 2). These nonlinear trends have not yet been followed to completion. We hope soon to resolve whether binary formation, disk fragmentation, or sustained nonlinear turbulence is the final outcome.

APPENDIX: NUMERICAL PERFORMANCE OF THE 3D HYDRODYNAMICS CODE

In Section 3, we report the dynamic growth of higher-order (up to $m = 5$), high-frequency ($\Omega_p \approx \Omega_{max}$) disturbances with short radial wavelengths (a few radial zones). This makes rather severe demands on the performance of the numerical scheme. In this Appendix, we report the results of several tests which estimate the code's numerical dissipation and diffusion.

One of the tests is the recomputation of a standard bar mode ($m = 2$) calculation. We choose $n = 3/2$, $n' = 0$, and $T/|W| = 0.33$ with a grid resolution similar to that in Tohline *et al.* (1985) and Durisen *et al.* (1986). As cited in Tohline *et al.*, for the bar mode, the tensor virial equations yield an approximate pattern speed Ω_p(TVE) = 0.019 and an e-folding time t_e(TVE) = 55 in polytrope units. Simulations done with their first-order 3D code give a pattern speed Ω_p(first) = 0.021 and an e-folding time t_e(first) = 120, as deduced from the Fourier amplitudes A_2 and phase ϕ_2. The difference between the inverses of t_e(TVE) and t_e(first) gives a numerical damping rate $1/t_d$, where t_d is the damping time. The observed damping time t_d(first) = 100 agrees within 10–20% with the damping time estimated from their code's truncation error. In terms of the shortest rotation period in the model, t_d(first) is about unity.

Using our present code, we obtain a pattern speed Ω_p(present) = 0.023 ± 0.001 and an e-folding time t_e(present) = 67 ± 10. The pattern speed agrees closely with Ω_p(first), suggesting that the true physical Ω_p for $m = 2$ is somewhat greater than Ω_p(TVE) by 15%. Comparison of t_e(TVE) with t_e(present) suggests t_d(present) = 300, or about three times the shortest rotation period, but with a 50% uncertainty. The improvement over first order is not as large as expected for a fully second-order scheme. The overall phase coherence of the bar in the present code is also not nearly as good as in the first-order calculations, and a sawtooth in the radial momentum density develops.

For $m = 4$, we expect t_d to be two to four times shorter than t_d for $m = 2$. In other words, for $m = 4$, t_d(present) should be about one rotation period. In the $T/|W| = 0.056$ protostellar core model, we do observe the $m = 4$ disturbances dying out on a time scale $t_d = 1.0 \pm 0.2$ in units of the shortest rotation period. Only instabilities with t_e less than one or two rotation periods can grow in our present code. In fact, we find that $m = 3$, 4, and 5 disturbances for which we detect growth in the $T/|W| = 0.157$ model all have t_e's shorter than a rotation period. For $m = 1$ and 2, we detect growth on e-folding times of one or two rotation periods.

As another test, we ran a calculation for the $T/|W| = 0.157$ model with the full $32 \times 64 \times 16$ grid but without an initial perturbation. After nearly two rotations, corresponding to 2500 time steps, the total energy of the model changed by 0.01%; the energy distribution among kinetic, internal, and gravitational shifted by about a percent mainly due to the model's oscillation about equilibrium. The $j(\mathcal{M})$ distribution, recalling $\mathcal{M}$ is mass within a cylindrical radius r, is indistinguishable at the present level between the initial and final times, suggesting that the time scale for angular momentum transport due to shear viscosity caused by numerical truncation error is longer than many tens of rotation periods. Even in the $T/|W| = 0.157$ calculation with $m = 1$ off, which ran for about seven rotations and developed large-scale nonaxisymmetry, no more than a few percent nonsystematic transport of J is evident comparing the initial and final $j(\mathcal{M})$ away from the rotation axis. For a few innermost zones which have less than 1 or 2% of J, j tends to become constant due to the large $\Delta r/r$ but is restricted to that region only.

The $T/|W| = 0.157$ protostellar core calculation without an initial perturbation also shows that nonaxisymmetric numerical noise does not grow rapidly from round-off error. On the Cray X-MP/48 at National Center for Supercomputing Applications, after 2500 steps, the Fourier amplitudes A_m are typically at a level of 10^{-14}, with largest values in a few zones of about 10^{-13} in $m = 4$ and 5. As a comparison, the expected round-off error is about 10^{-15}.

We consider the sawtooth behavior of the radial momentum density in the bar mode calculation disturbing. Such a sawtooth is also present in the $T/|W| = 0.157$ model, but is absent in the $T/|W| = 0.056$ case. Shifting the radial momentum density to a face-centered location cures the sawtooth but produces considerably greater numerical damping for $m \geq 3$ disturbances. We are continuing efforts to cure the sawtooth without sacrificing our ability to detect high-order modes at affordable resolution.

ACKNOWLEDGMENTS

Special thanks are due C. Yuan and F. C. Adams for valuable discussions and help. We also acknowledge useful discussions or correspondence with P. Bodenheimer, A. P. Boss, P. Cassen, D. Christodoulou, D. N. C. Lin, S. M. Miyama, F. K. Shu, J. E. Tohline, and H. A. Williams. We appreciate the assistance of J. S. Best with data analysis of the three-dimensional hydrodynamics calculation. This work was partially funded by NSF Grant AST 85-21272 and by allocations of supercomputer time from the National Center for Supercomputing Applications at the University of Illinois, Urbana–Champaign.

Note added in proof. Calculations currently underway with higher spatial resolution ($64 \times 64 \times 16$) do not exhibit a numerical sawtooth. For $T/|W| = 0.157$, dynamic nonaxisymmetric instabilities again occur but have lower growth rates and are dominated by $m = 1$ and 2 even in the linear regime. A mode similar to the $m = 4$ reported here is detected in the new calculation but is less vigorous. So, although details are somewhat sensitive to numerics, the fundamental conclusion that disks suffer dynamic nonaxisymmetric instabilities during their earliest stages of formation seems robust.

REFERENCES

ADAMS, F. C., AND D. N. C. LIN 1990. Transport process and the evolution of disks. In *Protostars and Planets III* (E. H. Levy and J. N. Lunine, Eds.). Univ. of Arizona Press, Tucson.

ADAMS, F. C., S. P. RUDEN, AND F. H. SHU 1989. Eccentric gravitational instabilities in nearly Keplerian disks. *Astrophys. J.* **347,** 959–975.

ADAMS, F. C., AND F. H. SHU 1986. Infrared spectra of rotating protostars. *Astrophys. J.* **308,** 836–853.

BECKWITH, S. V. W., AND A. I. SARGENT 1990. The occurrence and properties of disks. In *Protostars and Planets III* (E. H. Levy and J. I. Lunine, Eds.). Univ. of Arizona Press, Tucson.

BECKWITH, S. V. W., A. I. SARGENT, R. S. CHINI, AND R. GUSTEN 1990. A survey for circumstellar disks around young stellar objects. *Astron. J.* **99,** 924–945.

BINNEY, J., AND S. TREMAINE 1987. *Galactic Dynamics*. Princeton Univ. Press, Princeton, NJ.

BODENHEIMER, P., AND J. P. OSTRIKER 1973. Rapidly rotating stars. VIII. Zero-viscosity polytropic sequence. *Astrophys. J.* **180,** 159–169.

BOSS, A. P. 1989. Evolution of the solar nebula. I. Nonaxisymmetric structure during nebula formation. *Astrophys. J.* **345,** 554–571.

CASSEN, P., AND A. MOOSMAN 1981. On the formation and evolution of protostellar disks. *Icarus* **48,** 353–376.

CHANDRASEKHAR, S. 1969. *Ellipsoidal Figures of Equilibrium*. Yale Univ. Press, New Haven.

CHRISTODOULOU, D. M., AND J. E. TOHLINE 1990. *Using 3-D Numerical Hydrodynamics to Study the Dynamical Evolution of Stellar Accretion Disks*. Preprint. Louisiana State Univ., Baton Rouge.

DURISEN, R. H. 1975. Viscous effects in rapidly rotating stars with application to white-dwarf models. III. Further numerical results. *Astrophys. J.* **195,** 483–492.

DURISEN, R. H. AND R. A. GINGOLD 1986. Numerical simulations of fission. In *Origin of the Moon* (W. K. Hartmann, R. J. Phillips, and G. J. Taylor, Eds), pp. 487–498. Lunar and Planetary Inst., Houston.

DURISEN, R. H., R. A. GINGOLD, J. E. TOHLINE, AND A. P. BOSS 1986. Dynamic fission instabilities in rapidly rotating $n = 3/2$ polytropes. *Astrophys. J.* **305,** 281–308.

DURISEN, R. H., AND J. E. TOHLINE 1985. Fission of rapidly rotating fluid systems. In *Protostars and Planets II* (D. C. Black and M. S. Matthews, Eds.), pp. 534–575. Univ. of Arizona Press, Tucson.

DURISEN, R. H., S. YANG, P. CASSEN, AND S. W. STAHLER 1989. Numerical models of rotating protostars. *Astrophys. J.* **345,** 959–971.

FRIEDMAN, J. L., AND B. F. SCHUTZ 1978. Lagrangian perturbation theory of nonrelativistic fluids. *Astrophys. J.* **221,** 937–957.

HACHISU, I., J. E. TOHLINE, AND Y. ERIGUCHI 1988. Fragmentation of rapidly rotating gas clouds. II. Polytropes—Clues to the outcome of adiabatic collapse. *Astrophys. J. Suppl.* **66,** 315–342.

IMAMURA, J. N., J. L. FRIEDMAN, AND R. H. DURISEN 1985. Secular stability limits for rotating polytropic stars. *Astrophys. J.* **294,** 474–478.

IMAMURA, J. N., J. TOMAN, S. YANG, AND R. H. DURISEN 1990. In preparation.

LYNDEN-BELL, D., AND J. P. OSTRIKER 1967. On the stability of differentially rotating bodies. *Mon. Not. R. Astron. Soc.* **136,** 293–310.

MIYAMA, S. M., C. HAYASHI, AND S. NARITA 1984. Criteria for collapse and fragmentation of rotating, isothermal clouds. *Astrophys. J.* **279,** 621–632.

NORMAN, M. L., AND K.-H. A. WINKLER 1986. 2D Eulerian hydrodynamics with fluid interfaces, self-gravity and rotation. In *Astrophysical*

Radiation Hydrodynamics (K.-H. A. Winkler and M. L. Norman, Eds.), pp. 187–221. Reidel, Dordrecht.

OSTRIKER, J. P., AND J. W.-K. MARK 1968. Rapidly rotating stars. I. The self-consistent-field method. *Astrophys. J.* **151,** 1075–1088.

PAPALOIZOU, J. C. B., AND G. T. SAVONIJE 1989. Non-axisymmetric instabilities in thin self-gravitating differentially rotating gaseous disks. In *Dynamics of Astrophysical Disks* (J. A. Sellwood, Ed.), pp. 103–114. Cambridge Univ. Press. Cambridge.

SARGENT, A. I., AND S. BECKWITH 1987. Kinematics of the circumstellar gas of HL Tauri and R Monocerotis. *Astrophys. J.* **323,** 294–305.

SCHUTZ, B. F. 1979. General variational principle for normal modes of rotating stars. *Astrophys. J.* **232,** 874–877.

SELLWOOD, J. A. 1989. Spiral instabilities in N-body simulations. In *Dynamics of Astrophysical Disks* (J. A. Sellwood, Ed.), pp. 155–171. Cambridge Univ. Press, Cambridge.

SHU, F. H. 1977. Self-similar collapse of isothermal spheres and star formation. *Astrophys. J.* **214,** 488–497.

SHU, F. H., F. C. ADAMS, AND S. LIZANO 1987. Star formation in molecular clouds: Observation and theory. *Annu. Rev. Astron. Astrophys.* **25,** 23–81.

SHU, F. H., S. TREMAINE, F. C. ADAMS, AND S. P. RUDEN 1990. Sling amplification and eccentric gravitational instabilities in gaseous disks. *Astrophys. J.* **358,** 495–514.

STAHLER, S. W. 1988. Deuterium and the stellar birthline. *Astrophys. J.* **332,** 804–825.

STROM, S. 1990. Observations of disk dispersal: Timescales and possible constraints on planets. In *Protostars and Planets III* (E. H. Levy and J. I. Lunine, Eds.). Univ. of Arizona Press, Tucson.

TASSOUL, J.-L. 1978. *Theory of Rotating Stars*. Princeton Univ. Press, Princeton, NJ.

TOHLINE, J. E. 1980. Fragmentation of rotating protostellar clouds. *Astrophys. J.* **235,** 866–881.

TOHLINE, J. E., R. H. DURISEN, AND M. MCCOLLOUGH 1985. The linear and nonlinear dynamic stability of rotating $n = 3/2$ polytropes. *Astrophys. J.* **298,** 220–234.

TOOMRE, A. 1981. What amplifies the spirals? In *The Structure and Evolution of Normal Galaxies* (S. M. Fall and D. Lynden-Bell, Eds.), pp. 111–136. Cambridge Univ. Press, Cambridge.

VISHNIAC, E. T., AND P. DIAMOND 1989. A self consistent model of mass and angular momentum transport in accretion disks. *Astrophys. J.* **347,** 435–447.

WILLIAMS, H. A. 1988. *Star Formation, Using 3-D Explicit Eulerian Hydrodynamics*. Ph.D. thesis, Louisiana State Univ., Baton Rouge.

WILLIAMS, H. A., AND J. E. TOHLINE 1987. Linear and nonlinear dynamic instability of rotating polytropes. *Astrophys. J.* **315,** 594–601.

WILLIAMS, H. A., AND J. E. TOHLINE 1988. Circumstellar ring formation in rapidly rotating protostars. *Astrophys. J.* **334,** 449–464.

YANG, S., AND R. H. DURISEN 1989. A dynamic $m = 1$ instability in rapidly rotating, low-mass protostar models. *Bull. Amer. Astron. Soc.* **21,** 794.

YUAN, C., AND P. CASSEN 1985. Protostellar angular momentum transport by spiral density waves. *Icarus* **64,** 435–447.